Available online at www.sciencedirect.com
ScienceDirect
Trans. Nonferrous Met. Soc. China 31(2021) 2153−2164
Transactions of Nonferrous Metals Society of China
www.tnmsc.cn

Formation of arsenic−copper-containing particles and their sulfation decomposition mechanism in copper smelting flue gas

Wen-ming YAO[1], Xiao-bo MIN[1,2], Qing-zhu LI[1,2], Kai-zhong LI[1], Yun-yan WANG[1], Qing-wei WANG[1,2,3], Hui LIU[1,2], Sheng-li QU[3], Zhun-qin DONG[3], Chao QU[3], Tao CHEN[3], Chao SONG[4]

1. School of Metallurgy and Environment, Central South University, Changsha 410083, China;
2. National Engineering Research Center for Control & Treatment of Heavy Metal Pollution, Central South University, Changsha 410083, China;
3. Shandong Humon Smelting Co., Ltd., Yantai 264109, China;
4. Yantai Humon Group Co., Ltd., Yantai 264100, China

Received 26 January 2021; accepted 7 June 2021

Abstract: The heat recovery steam generator (HRSG) of copper smelting generates a large number of arsenic−copper-containing particles, and the in-situ separation of arsenic and copper is of importance for cutting off environmental risk and realizing resource recovery. The formation of arsenic−copper-containing particles was simulated, the method of in-situ decomposition of arsenic−copper-containing particles by pyrite was proposed, and the decomposition mechanism was confirmed. It was found that particles with high arsenic content were formed in the simulated HRSG, and copper arsenate was liable for the high arsenic content. Pyrite promoted the sulfation of copper, leading to the in-situ decomposition of copper arsenate. In this process, gaseous arsenic was released, and thus the separation of arsenic and copper was realized.

Key words: copper smelting flue gas; particles; sulfation decomposition; copper arsenate; pyrite

1 Introduction

Arsenic is a ubiquitous contaminant in the environment through geochemical migration and industrial production activities [1−3]. It is seen as the most hazardous waste material on the basis of the USEPA agency [4]. Arsenic contamination caused by copper smelting has attracted growing public attention due to its toxicity and potential health threat [5−7]. In copper smelting system, 60% of arsenic is oxidized to vapor phase of arsenic trioxide (As_2O_3(g)), creating arsenic-containing flue gas [8]. The collection of arsenic trioxide in the smelting flue is the key to the directional control of arsenic [9]. The most commonly used means is to set quench tower after heat recovery steam generator (HRSG) [10]. Considering the high copper content (up to 40%) [11] in the dust of HRSG, the arsenic−copper-containing particles are further formed. This arsenic-containing material in turn reduces the arsenic capture rate in the quench tower. In addition, the dust of HRSG is always recycled into the smelting circuit. While this method is appropriate for the recovery of copper, the existence of injurious arsenic leads to subsequent contamination of cathode copper products [11]. With increasing the content of arsenic in copper mineral, the issue brings about a dilemma for future copper industry in terms of health exposure as well as copper grade. Therefore, the efficient separation of arsenic and copper in the dust of HRSG has been an increasingly pressing mission in sustainable engineering of copper smelting.

Corresponding author: Qing-zhu LI, Tel: +86-731-89875182, E-mail: qingzhuli@csu.edu.cn
DOI: 10.1016/S1003-6326(21)65645-5

However, the current pyrometallurgy separation of arsenic in smelting dust is mainly limited to open-circuit treatment, that is, to handle the particles that have been transported out of the smelting flue. The addition of reducing agents (such as activation carbon, elemental sulfur, and CuS) can release arsenic trioxide from the dust [12]. However, reassembly of heat treatment facility and management of arsenic-containing substances increased costs and risks of open-circuit treatment. Additionally, the open-circuit processing techniques cannot be directly applied to in-situ decomposition of arsenic−copper-containing particles in HRSG because high concentrations of sulfur dioxide (SO_2) and oxygen (O_2) in copper metallurgical gas are not considered. Thus, the separation of arsenic and copper in HRSG is a novel area that requires further research.

Pyrite (FeS_2) is one of the most abundant sulfide minerals in curst, and is widely used for heavy metal phase control in high temperature process. Therefore, pyrite has attracted widespread attention in improving the surface properties of metal oxides. For instance, ZHENG et al [13] and LIU et al [14] proved that surface sulfurization of zinc oxide could be realized by pyrite at high temperature. ZHENG et al [15] researched the surface sulfurization performance of lead oxide by pyrite in baking process. Moreover, pyrite could be oxidized to magnetite under oxidative roasting, and this oxidized product has less adsorption capacity for arsenic [16]. Based on these advantages, surface sulfurization of copper by pyrite may be an economically reasonable and scientifically feasible solution for separating arsenic and copper in HRSG. However, surface sulfurization technology is limited in HRSG because of its strict requirements on inert atmosphere or weak reducing atmosphere. Taking full account of the SO_2−O_2 atmosphere of the HRSG, surface sulfation of copper may be a suitable technology for the separation of copper and arsenic in HRSG. Unfortunately, the detailed investigation is extremely rare in literatures.

This study aims at achieving the valid separation of copper and arsenic in dust of the simulated HRSG. To reach this goal, the influence of sulfur dioxide (SO_2) and oxygen (O_2) concentration on the formation of arsenic−copper-containing particles in the simulated HRSG is discussed. Then, the sulfation method based on pyrite is proposed for separating arsenic and copper in smelting dust. Furthermore, the sulfation decomposition mechanism of arsenic−copper-containing particles is explored in depth. It is anticipated that the study will provide an important theoretical reference for scientific disposal of arsenic-containing particles.

2 Experimental

2.1 Materials

The arsenic trioxide (As_2O_3) was collected from Shandong Humon Smelting Co., Ltd., China. The content of arsenic trioxide (98.71%) was determined by the analysis of inductively coupled plasma optical emission spectrometry (ICP-OES). Pyrite (FeS_2) derived from a natural mineral was detected by the X-ray diffractometer (XRD), which exhibited high crystallinity and purity (Fig. 1). The chemicals used in this study, including copper oxide (CuO), copper sulfate ($CuSO_4$ and $CuSO_4·5H_2O$), hydrochloric acid (HCl), hydrogen nitrate (HNO_3), and sodium hydroxide (NaOH) were of analytical grade, and were purchased from Sinopharm Group Chemical Reagent Co., Ltd., China. The silica filter (No. 88RH) was gained from Advantec Shanghai Office, China. Standard solution of arsenic used for detection was obtained from General Research Institute for Nonferrous Metals, China.

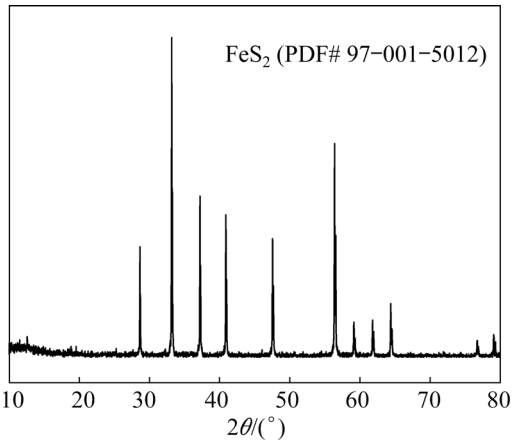

Fig. 1 XRD pattern for pyrite used in experiment

2.2 Simulated HRSG apparatus and batch tests

The formation and sulfation decomposition of arsenic−copper-containing particles were investigated in a simulated HRSG apparatus, as shown in Fig. 2. The simulated HRSG primarily consisted of gasholder, mass flow meters, flow

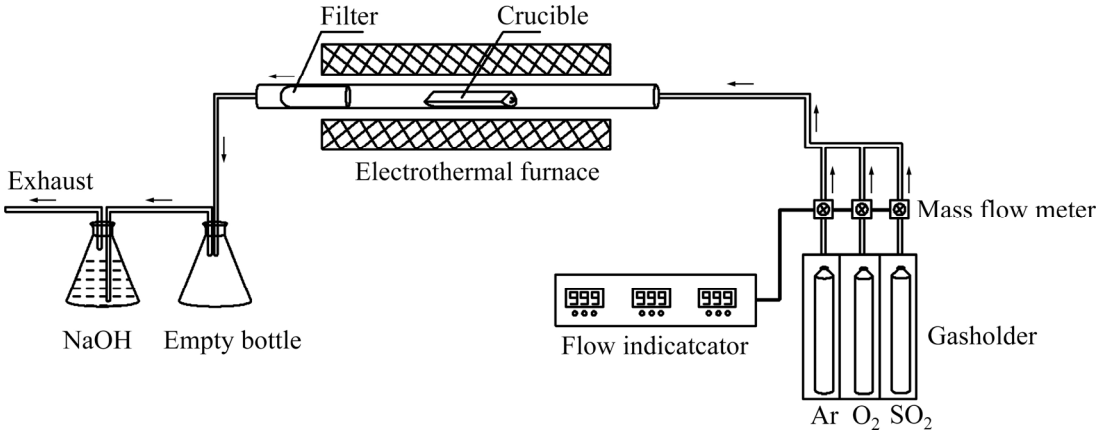

Fig. 2 Schematic diagram of simulated HRSG apparatus

indicator, and electrothermal furnace. The gasholder, mass flow meters, and flow indicator were used to provide a mixture of sulfur dioxide, oxygen, and argon (Ar). Electrothermal furnace was utilized to heat samples, with constant temperature zone of 300 mm. The uniform mixture of arsenic trioxide, copper oxide, and pyrite was put into a quartz crucible. The quartz crucible containing sample and the silica filter referred to the literatures [17,18] were put into a quartz tube. Once the electrothermal furnace was heated up to 873 K, the quartz tube was quickly pushed to the constant temperature zone. SO_2 and O_2 were introduced into the quartz tube according to the flow rate designed in the test. Argon was applied as a supplementary and protective gas. The gas mixtures of 100 mL/min flowed to the quartz tube in the direction indicated by the arrow. In order to avert grievous environmental pollution caused by the off-gas, the silica filter and the sodium hydroxide solutions were adopted to collect quenched arsenic-containing particles and to absorb gaseous arsenic, respectively. The empty bottle prevented the sodium hydroxide solution from being sucked back. The reaction time at constant temperature zone was 1 h for each test. The arsenic−copper-containing particles corresponding to the HRSG were produced in the quartz crucible.

The influence of SO_2 and O_2 concentration on the formation of arsenic−copper-containing particles in the simulated HRSG was investigated. The pretreated sample consisting of arsenic trioxide and copper oxide with a mass ratio of 1:1 and a total of 5.00 g was required for each test. The influence of SO_2 concentration (0%, 20%, 40%, 60% and 80%) on arsenic content and phase structure was examined in the arsenic−copper-containing particles in 20% O_2. Similarly, the effect of O_2 was also determined by adjusting the concentration of oxygen (0%, 20%, 40%, 60% and 80%) in 20% SO_2.

The sulfation separation of arsenic and copper in the arsenic−copper-containing particles was conducted to assess the effects of pyrite. The concentration of sulfur dioxide and oxygen was determined to be 20% based on the composition characteristics of copper pyrometallurgy off-gas. The mixture composition contains 2.50 g arsenic trioxide, 2.50 g copper oxide, and a certain amount of pyrite, as given in Table 1.

Table 1 Composition of mixture

Sample	*m*(Copper oxide)/g	*m*(Arsenic trioxide)/g	*m*(Pyrite)/g	Pyrite dosage/%
W_0	2.50	2.50	0	0
W_1	2.50	2.50	1.00	20
W_2	2.50	2.50	2.00	40
W_3	2.50	2.50	3.00	60
W_4	2.50	2.50	4.00	80
W_5	2.50	2.50	5.00	100

2.3 Characterization

The crystal structures of arsenic−copper-containing particles were detected by XRD (Siemens D5000) using Cu K_α radiation and scanning speed of 10 (°)/min. The arsenic content was characterized by ICP-OES (ICAP7400 Radial). The surface microscopic morphology and chemical structure of the particles formed were determined

by scanning electron microscopy (SEM, Zeiss-SIGMAHD) and Fourier transform infrared spectroscopy (FTIR, Bruker TENSOR 27). The elements and valence state of sample surface were detected by X-ray photoelectron spectroscopy (XPS, Thermo Fisher Scientific) equipped with Al K_α X-ray as the excitation source. The C 1s peak at 284.8 eV was used to calibrate all the obtained binding energies.

3 Result and discussion

3.1 Formation of arsenic−copper-containing particles

Before designing in-situ separation scheme of arsenic and copper in the arsenic−copper-containing particles, it is necessary to understand the formation mechanism of particles in the smelting atmosphere with SO_2 and O_2.

The influence of SO_2 concentration on arsenic content and phase structure of the formed particles was analyzed using ICP-OES and XRD at O_2 concentration of 20%, as shown in Fig. 3. Figure 3(a) illustrates that the arsenic content held at a relatively high level of 26.33%−30.12%, larger than the arsenic content (5%−18%) in actual dust of existing HRSG. It is indicated that copper oxide could react with arsenic trioxide at different SO_2 concentrations. It is worthy to point out that the arsenic content showed a weak downward trend (i.e., <4% difference) as SO_2 concentration increased from 0 to 80%. In order to reveal the reason for this subtle change in arsenic content, XRD was used to analyze the phases of arsenic−copper-containing particles in Fig. 3(b). Copper arsenate ($Cu_3(AsO_4)_2$) was the only arsenic-containing phase, whereas there were many other copper-containing phases, including copper oxide (CuO), dolerophane ($Cu_2O(SO_4)$), copper sulfate ($CuSO_4$ and $CuSO_4·5H_2O$). With the enhancement of SO_2 concentration, the diffraction peak intensity of copper-containing phase changed significantly, that is, the peak intensity of copper arsenate decreased while the peak intensity of the dolerophane and copper sulfate increased. It can be concluded that SO_2 promoted the formation of sulfation (copper sulfate and dolerophane) and weakened the formation of copper arsenate, decreasing the arsenic content of the particles. Unfortunately, sulfation degree caused by SO_2 was relatively weak, which can only lead to a small reduction (less than 4%) of arsenic content in the arsenic−copper-containing particles. Therefore, further study on sulfation is still needed.

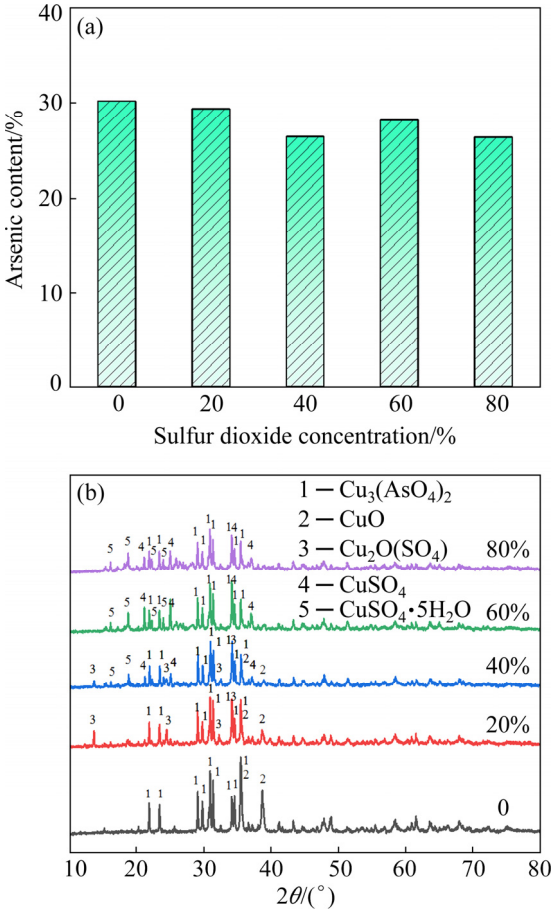

Fig. 3 Arsenic content (a) and XRD patterns (b) of arsenic−copper-containing particles with different SO_2 concentrations

Similarly, the influence of O_2 concentration on arsenic content and phase structure of the particles was tested at SO_2 concentration of 20%, and the results are shown in Fig. 4. In Fig. 4(a), the arsenic content in arsenic−copper-containing particles increased significantly from 22.42% to 43.15% when O_2 concentration was improved from 0 to 80%. Obviously, copper oxide could also react with arsenic trioxide at different O_2 concentrations. Compared with the changes in arsenic content (i.e., <4% difference) caused by SO_2, the variation in arsenic content (i.e., >20% difference) caused by O_2 was larger. Therefore, O_2 seemed to be more conducive to the formation of arsenic-containing particles than SO_2. In order to reveal the reason for the significant increase of arsenic content, XRD was used to analyze the phases of arsenic−

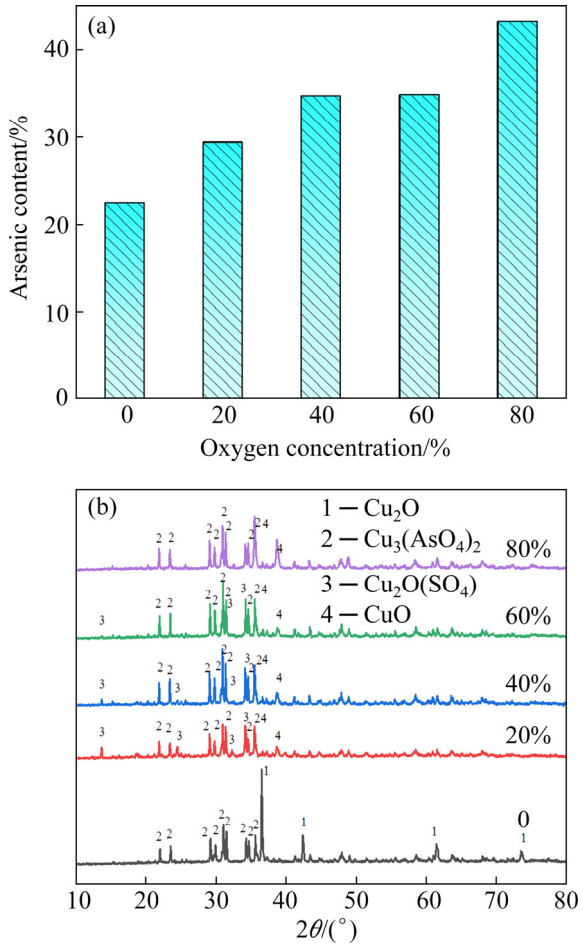

Fig. 4 Arsenic content (a) and XRD patterns (b) of arsenic−copper-containing particles with different O_2 concentrations

copper-containing particles, as shown in Fig. 4(b). It can be found that the characteristic peaks of copper arsenate and copper oxide were strengthened gradually when O_2 concentration increased from 0 to 80%. Although the formation of dolerophane and copper sulfate was also found in the presence of O_2, these peaks were weakened gradually with the increment of O_2 concentration. Hence, it can be concluded that there was a competition between the formation of copper-containing sulfate (i.e. dolerophane and copper sulfate) and copper arsenate under O_2 atmosphere. Additionally, the lower concentration of O_2 was beneficial to the sulfation of copper, thus forming particles with low arsenic content. Nevertheless, when O_2 was not available, it was disadvantageous to the formation of copper-containing sulfation. At the same time, copper arsenate can be formed through the reaction of arsenic trioxide and copper oxide, where copper oxide was reduced to cuprous oxide (Cu_2O) to provide oxygen. As a result, it was impossible to reach a high sulfation degree that can separate arsenic from arsenic−copper-containing particles by regulating O_2 concentration.

From the analysis above, copper arsenate was the only arsenic-containing phase and was responsible for the high arsenic content in the arsenic−copper-containing particles. The formation of copper-containing sulfate could be promoted by regulating the concentration of sulfur dioxide and oxygen, resulting in in-situ decomposition of copper arsenate and reducing the arsenic content in the arsenic−copper-containing particles. Because the formation of copper arsenate and copper-containing sulfate was a competitive process, it can be speculated that if the sulfation transformation of copper is strengthened, the formation of copper arsenate would be correspondingly reduced, thus contributing to the separation of copper and arsenic. However, the reduction of arsenic content is limited by regulating the concentrations of sulfur dioxide and oxygen. Hence, it is necessary to strengthen the sulfation of copper in order to effectively separate arsenic and copper in the HRSG of copper smelting flue.

3.2 Sulfation decomposition of arsenic−copper-containing particles

Pyrite has attracted widespread attention in surface sulfurization of heavy metals in an inert or reducing atmosphere, and pyrite is usually converted to FeS or FeS_x ($0<x<1$) in the sulfurization process. However, the HRSG has unique and complex sulfur dioxide and oxygen environment, which may affect the chemical reaction of pyrite. Hence, the sulfation separation of arsenic and copper using pyrite is proposed for the first time, and its mechanism is confirmed in terms of the analyses of ICP-OES, SEM, XRD, FTIR and XPS.

The impact of pyrite dosages on separation of arsenic and copper in the arsenic−copper-containing particles is displayed in Fig. 5. The arsenic content in the particles decreased significantly (i.e., from 29.31% to 4.89%) when the pyrite dosage was increased from 0 to 40%, and then decreased slightly to the minimum value of 2.47% when the pyrite dosage was more than 40%. Clearly, pyrite could effectively separate the arsenic and copper in the particles of the simulated HRSG.

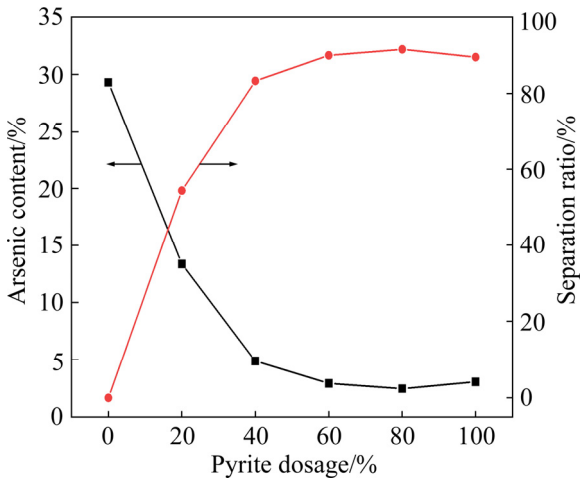

Fig. 5 Effect of pyrite dosages on decomposition of arsenic−copper-containing particles

After comprehensive consideration, the optimal dosage of pyrite was determined to be 60%. At the same time, arsenic content and separation ratio were 2.93% and 90.02%, respectively.

Figure 6 depicts the morphologies of particles before and after the separation of arsenic and copper. Before separation, as shown in Figs. 6(a, b), Sample W_0 consisted of a large quantity of plate-like particles with smooth surface, clear boundaries and large sizes (100−500 nm), which belonged to micron-sized copper arsenate particles. After separation of copper and arsenic (Figs. 6(c, d)), Sample W_5 exhibited a completely different morphology, where sphere-like rough particles were observed with small diameter of about 20 nm, and the grain boundary became blurred, which implies the decomposition of copper arsenate.

Figure 7(a) reveals the phase composition change of arsenic−copper-containing particles with different pyrite dosages. When pyrite was not available (Sample W_0), there were three main phases in the particles, including copper arsenate, copper-containing sulfate, and copper oxide. With the addition of 20% pyrite, the peaks of copper arsenate and copper oxide were weakened rapidly; however, the peak intensities of copper-containing sulfate were increased. As shown in Sample W_2 with 40% pyrite, the peaks of copper arsenate disappeared while those for copper-containing sulfate, ferric oxide (Fe_2O_3) and magnetite (Fe_3O_4) were significantly enhanced. Combined with the separation ratio in Fig. 5, since copper was sulfated by pyrite, copper arsenate was in-situ decomposed, thereby achieving the separation of arsenic and copper. When pyrite dosage was increased to 60%, the peaks of the chalcopyrite-like product $(Cu_5Fe_2S_4)_{0.5}$ [19] appeared, implying the excessive

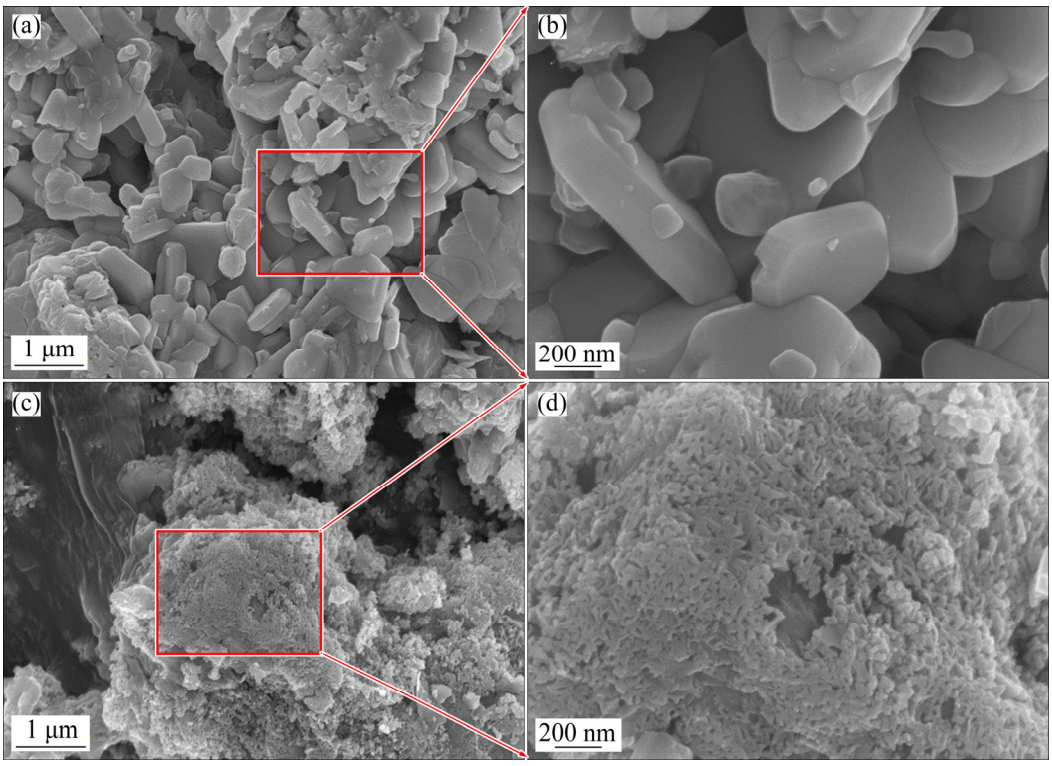

Fig. 6 SEM images of arsenic−copper-containing particles before (a, b) and after (c, d) separation

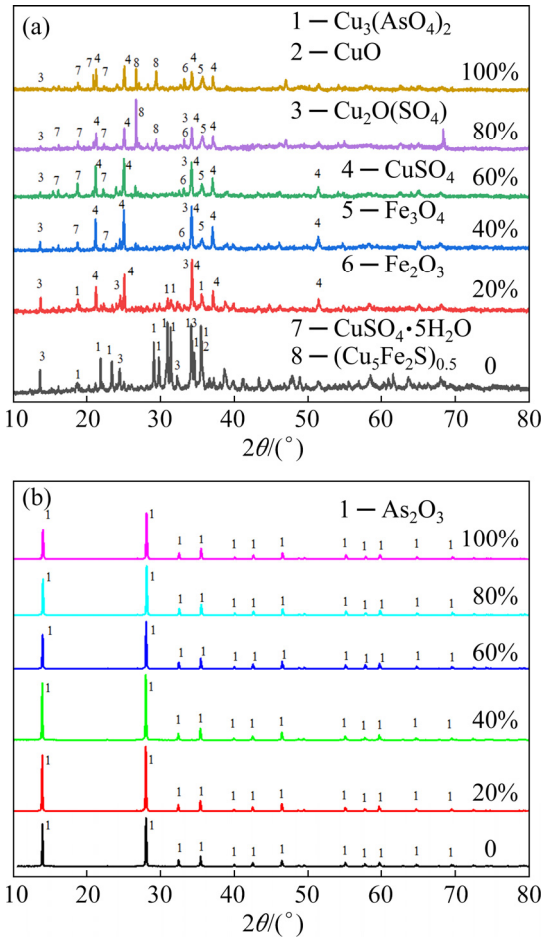

Fig. 7 XRD patterns of arsenic−copper-containing particles (a) and arsenic-containing particles (b) formed by condensation with different pyrite dosages

use of pyrite. Figure 7(b) illustrates the XRD patterns of arsenic-containing particles condensed in the silica filter. Only peaks of arsenolite (As_2O_3) were present after sulfation decomposition of copper arsenate, confirming that arsenic was released in the phase of arsenic trioxide, without oxidization further. Hence, the following reactions may occur:

$$3CuO+As_2O_3(g)+O_2(g)=Cu_3(AsO_4)_2 \quad (1)$$

$$2CuO+2SO_2(g)+O_2(g)=2CuSO_4 \quad (2)$$

$$3CuO+2SO_2(g)+O_2(g)=2Cu_2O(SO_4) \quad (3)$$

$$3FeS_2+2Cu_3(AsO_4)_2+9O_2(g)=2As_2O_3(g)+6CuSO_4+Fe_3O_4 \quad (4)$$

$$3FeS_2+4Cu_3(AsO_4)_2+7O_2(g)=4As_2O_3(g)+6Cu_2O(SO_4)+Fe_3O_4 \quad (5)$$

$$2FeS_2+1.33Cu_3(AsO_4)_2+6.17O_2(g)=1.33As_2O_3(g)+4CuSO_4+Fe_2O_3 \quad (6)$$

$$2FeS_2+2.67Cu_3(AsO_4)_2+4.83O_2(g)=2.67As_2O_3(g)+4Cu_2O(SO_4)+Fe_2O_3 \quad (7)$$

$$2FeS_2+1.67Cu_3(AsO_4)_2=1.67As_2O_3(g)+4.17O_2+8(Cu_5Fe_2S_4)_{0.5} \quad (8)$$

Generally speaking, a free sulfate (SO_4^{2-}) ion has T_d symmetrical characteristic, and four fundamental vibrating modes: nondegenerate mode (ν_1) at 965−981 cm^{-1}, doubly degenerate mode (ν_2) at 451−472 cm^{-1}, and two triply degenerate modes (ν_3 and ν_4) at 1060−1200 cm^{-1} and 590−630 cm^{-1}, respectively [20−23]. The structure of pure copper sulfate ($CuSO_4$) was determined by FTIR in Fig. 8.

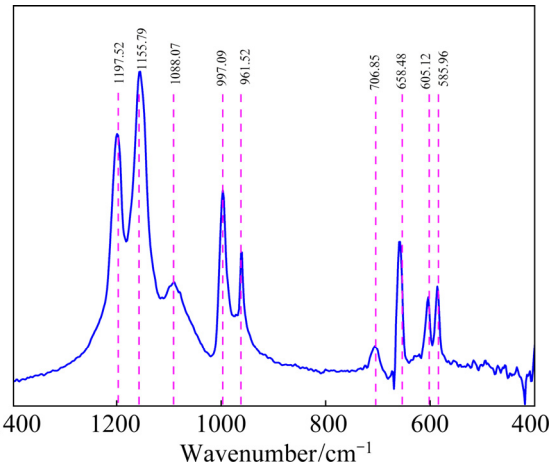

Fig. 8 FTIR spectrum of pure copper sulfate

The bands appearing at 1197.52, 1155.79 and 1088.07 cm^{-1} on the spectrum should be resulted from the triply degenerate symmetric stretching mode (ν_3) of SO_4^{2-}. The bands at 997.09 and 961.52 cm^{-1} were reasonably attributed to the non-degenerate mode (ν_1) of SO_4^{2-}. The bands at 706.85, 658.47, 605.12 and 585.96 cm^{-1} were ascribed to the mode (ν_4) of triply degenerate vibrations. No obvious doubly degenerate mode (ν_2) of SO_4^{2-} was found. According to the published literatures, the characteristic peaks of Fe—O usually emerge at 580−592 cm^{-1} [24−27], and the peaks of As—O usually appear at 782−855 cm^{-1} [28−31]. The FTIR spectrum showed no band related to stretching and bending vibrations of S—S. In the previous reports, the relevant absorption peaks of S—S were always observed in the wavenumber range of 414−612 cm^{-1} [20, 32].

In this study, FTIR spectra of arsenic−copper-containing particles with different pyrite dosages are displayed in Fig. 9. The peaks appearing at 1197.61, 1151.57 and 1093.96 cm^{-1} were reasonably assigned as the triply degenerate

symmetric stretching mode (ν_3) of SO_4^{2-}. The bands situated approximately at 995.35 and 964.07 cm^{-1} were all attributed to the non-degenerate mode (ν_1) of SO_4^{2-}. The peaks emerging at 696.32, 656.62, 604.75, and 586.18 cm^{-1} should be ascribed to the triply degenerate mode (ν_4) of SO_4^{2-}, and the band at 478.61 cm^{-1} should be assigned to the doubly degenerate mode (ν_2) of SO_4^{2-}. These findings were in good agreement with the main characteristic peaks of copper sulfate. According to Fig. 7, these characteristic peaks were related to the presence of dolerophane and copper sulfate. The peaks located at 573.05 and 809.66 cm^{-1} were attributed to the Fe—O and As—O, respectively. As—O band was stemmed from copper arsenate, and Fe—O band from ferric oxide and magnetite. The 553.53 and 457.48 cm^{-1} bands belonged to the S—S functional group, which were assigned to the chalcopyrite-like product. The FTIR band of As—O was obvious as pyrite was absent, but disappeared as pyrite dosage was enhanced to 40% or more. Meanwhile, the absorbance of bands of Fe—O and SO_4^{2-} increased gradually. These all demonstrated that pyrite achieved the separation of arsenic and copper by promoting the sulfation of copper and the in-situ decomposition of copper arsenate, while iron atoms were oxidized to ferric oxide or magnetite. The presence of S—S bond of the chalcopyrite-like product implied an excess use of pyrite.

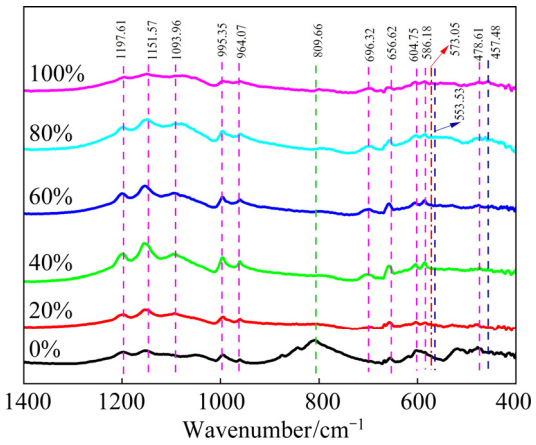

Fig. 9 FTIR spectra of arsenic−copper-containing particles with different pyrite dosages

Figure 10 shows the XPS spectra of arsenic−copper-containing particles with different pyrite dosages. As can be seen from Fig. 10(a), the arsenic−copper-containing particles mainly contained Cu, Fe, O, S and As elements, being consistent with XRD results. In Fig. 10(b), Cu $2p_{3/2}$ was fitted with two characteristic peaks located at 935.15 and 932.74 eV, respectively. According to the Cu $2p_{3/2}$ spectra in copper oxide, synthetic copper arsenate and dolerophane in Fig. 11, the binding energies at 935.46, 935.40, 934.08 and 932.59 eV in Cu $2p_{3/2}$ scan corresponded to copper sulfate, copper arsenate, copper oxide, and dolerophane, respectively [33−36]. Thus, the 935.15 eV peak corresponded to copper sulfate, copper arsenate, and copper oxide, while the 932.74 eV peak was assigned to dolerophane and chalcopyrite-like product. As pyrite dosage increased from 0 to 40%, the peak at 935.15 eV experienced no shift and was weakened gradually. Combined with the XPS analyses of S 2p in Fig. 10(e) and As 3d in Fig. 10(f), this trend was attributed to the presence of copper sulfate and the reduction of copper arsenate and copper oxide. When pyrite dosage was 40%, copper arsenate disappeared completely, leaving copper sulfate and dolerophane. This result indicated that sulfation of copper mainly occurred under the action of pyrite, while copper arsenate was decomposed. Moreover, the peak at 932.74 eV showed a significant improvement as pyrite dosage increased from 60% to 100%, which was related to the appearance of the chalcopyrite-like product.

After adding pyrite, the peak appearing at 710.88 eV in Fig. 10(c) corresponded to the Fe $2p_{3/2}$, thereby showing the formation of ferric oxide and magnetite, which were consistent with the literatures [26,37−39]. However, these spectra never exhibited characteristic peak (at 708.2 eV) of bulk pyrite, indicating that pyrite was completely oxidized to ferric oxide and magnetite [16,40,41].

The O 1s peak at 531.93 eV in Fig. 10(d) was ascribed to the copper sulfate, copper arsenate and dolerophane, while the peak at 530.03 eV was assigned to the metallic oxide, such as copper oxide, ferric oxide and magnetite [42,43]. The peak at 530.03 eV got stronger with pyrite dosage increasing from 0 to 100%, which was linked to the increase of ferric oxide and magnetite contents.

According to the previous studies [38,44,45], the bands at 162.22 and 168.80 eV in Fig. 10(e) corresponded to the S—S functional group of the chalcopyrite-like product and the SO_4^{2-} functional group of copper sulfate, respectively. The band at 169.98 eV was ascribed to the SO_4^{2-} functional

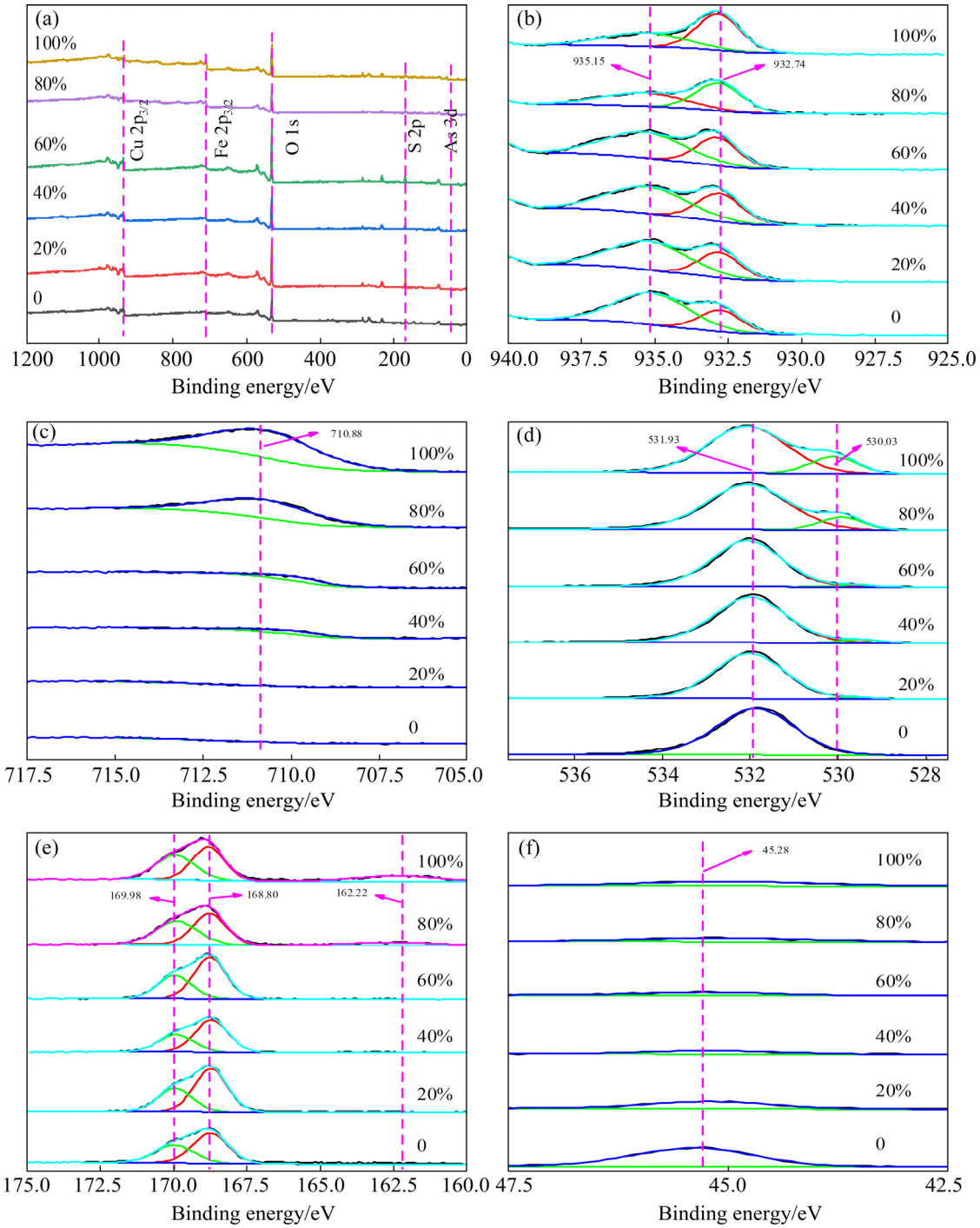

Fig. 10 XPS spectra for survey (a), Cu $2p_{3/2}$ (b), Fe $2p_{3/2}$ (c), O 1s (d), S 2p (e) and As 3d (f) of arsenic−copper-containing particles with different pyrite dosages

group of dolerophane. This showed that both copper sulfate and dolerophane coexisted, and the mass ratio of the two phases was relatively stable. With the increment of pyrite dosage, both copper sulfate and dolerophane increased in almost the same proportion. For instance, the content of copper sulfate increased from 60.59% to 63.95% and the content of dolerophane was from 36.05% to 39.41%, with pyrite dosage increasing from 0 to 60%. Besides, S^{2-} functional group of the chalcopyrite-like product appeared with pyrite dosage increasing from 80% to 100%, and its peak intensity increased with the increasing pyrite dosage [46]. This tendency was consistent with that of Cu $2p_{3/2}$. The reason for this change was the excessive use of pyrite.

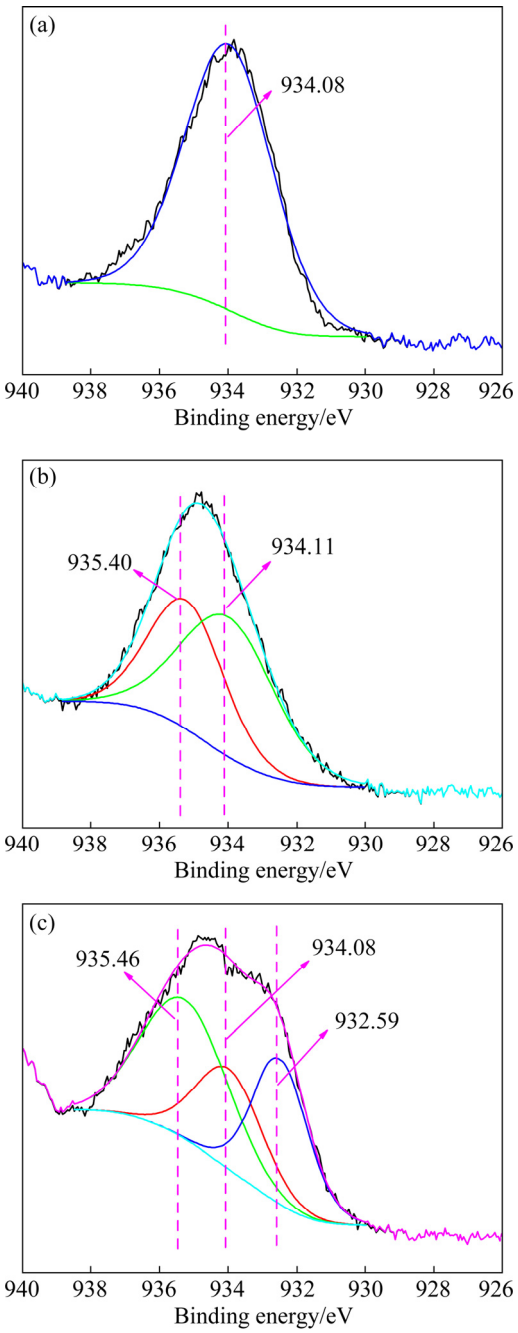

Fig. 11 XPS spectra for Cu $2p_{3/2}$ of copper oxide (a), synthetic copper arsenate (b) and dolerophane (c)

4 Conclusions

(1) The arsenic−copper-containing particles with high arsenic content were formed in a simulated HRSG. Copper arsenate ($Cu_3(AsO_4)_2$) was the only arsenic-containing phase in the particles and contributed to the high arsenic content.

(2) Sulfation of copper and arsenation of copper was a competitive process. However, the separation of arsenic and copper cannot be realized by SO_2−O_2 regulation in terms of sulfation degree of copper and the reduction of arsenic in particles.

(3) The pyrite dosage enhanced the sulfation degree of copper and promoted the in-situ decomposition of copper arsenate, achieving the separation of copper and arsenic in the simulated HRSG. Simultaneously, pyrite was oxidized to ferric oxide and magnetite.

(4) With the excessive use of pyrite, however, the chalcopyrite-like product $(Cu_5Fe_2S_4)_{0.5}$ was formed, so pyrite dosage should be controlled within a reasonable range.

Acknowledgments

This work was financially supported by the National Science Fund for Excellent Young Scholars of China (No. 52022111), the National Key Research and Development Program of China (Nos. 2017YFC0210401, 2018YFC1900306), the Distinguished Young Scholars of China (No. 51825403), and the National Natural Science Foundation of China (Nos. 51634010, 51974379).

References

[1] SAXENA G, KISHOR R, BHARAGAVA R. Bioremediation of industrial waste for environmental safety [M]. Singapore: Springer, 2020.

[2] CHAI Li-yuan. Arsenic pollution control in nonferrous metallurgy [M]. Singapore: Springer, 2019.

[3] XU Hui, MIN Xiao-bo, WANG Yun-yan, KE Yong, YAO Li-wei, LIU De-gang, CHAI Li-yuan. Stabilization of arsenic sulfide sludge by hydrothermal treatment [J]. Hydrometallurgy, 2020, 191: 105229.

[4] BOWELL R J, ALPERS C N, JAMIESON H E, NORDSTROM D K, MAJZLAN J. The environmental geochemistry of arsenic—An overview [J]. Reviews in Mineralogy and Geochemistry, 2014, 79(1): 1−16.

[5] ALI W, RASOOL A, JUNAID M, ZHANG H. A comprehensive review on current status, mechanism, and possible sources of arsenic contamination in groundwater: A global perspective with prominence of Pakistan scenario [J]. Environmental Geochemistry and Health, 2019, 41: 737−760.

[6] MANAY N, PISTON M, CACERES M, PIZZORNO P, BUHL V. An overview of environmental arsenic issues and exposure risks in Uruguay [J]. Science of the Total Environment, 2019, 686: 590−598.

[7] LI Yuan-cheng, MIN Xiao-bo, KE Yong, LIU De-gang, TANG Chong-jian. Preparation of red mud-based geopolymer materials from MSWI fly ash and red mud by mechanical activation [J]. Waste Manage, 2019, 83: 202−208.

[8] MONTENEGRO V, SANO H, FUJISAWA T. Recirculation of high arsenic content copper smelting dust to smelting and converting processes [J]. Minerals Engineering, 2013, 49: 184−189.

[9] DALEWSKI F. Removing arsenic from copper smelter gases [J]. International Journal of Minerals, Metallurgy and Materials, 1999, 51: 24−26.

[10] NAZARI A M, RADZINSKI R, GHAHREMAN A. Review of arsenic metallurgy: Treatment of arsenical minerals and the immobilization of arsenic [J]. Hydrometallurgy, 2017, 174: 258−281.

[11] JAROSIKOVA A, ETTLER V, MIHALJEVIC M, DRAHOTA P, CULKA A, RACEK M. Characterization and pH-dependent environmental stability of arsenic trioxide-containing copper smelter flue dust [J]. Journal of Environmental Management, 2018, 209: 71−80.

[12] ZHONG Da-peng, LI Lei. Separation of arsenic from arsenic−antimony-bearing dust through selective oxidation−sulfidation roasting with CuS [J]. Transactions of Nonferrous Metals Society of China, 2020, 30: 223−235.

[13] ZHENG Yong-xing, LV Jin-fang, WANG Hua, WEN Shu-ming, PANG Jie. Formation of zinc sulfide species during roasting of ZnO with pyrite and its contribution on flotation [J]. Scientific Reports, 2018, 8: 7839.

[14] LIU Wei, ZHU Lin, HAN Jun-wei, JIAO Fen, QIN Wen-qing. Sulfidation mechanism of ZnO roasted with pyrite [J]. Scientific Reports, 2018, 8: 9516.

[15] ZHENG Yong-xing, LV Jin-fang, WANG Hua, WEN Shu-ming, HUANG Ling-yun. Efficient sulfidization of lead oxide at high temperature using pyrite as vulcanizing reagent [J]. Physicochemical Problems of Mineral Processing, 2018, 54: 270−277.

[16] LIU Zhi-lou, YANG Shu, LI Zi-liang, XIE Xiao-feng, LI Yu-hu, SUN Zhu-mei, LUO Shuang, XU Zhi-feng. Three-layer core-shell magnetic Fe_3O_4@C@Fe_2O_3 micro-particles as a high-performance sorbent for the capture of gaseous arsenic from SO_2-containing flue gas [J]. Chemical Engineering Journal, 2019, 378: 122075.

[17] SONG Wen-jia, JIAO Fa-cun, YAMADA N, NINOMIYA Y, ZHU Zi-bin. Condensation behavior of heavy metals during oxy-fuel combustion: Deposition, species distribution, and their particle characteristics [J]. Energy and Fuels, 2013, 27: 5640−5652.

[18] YAO Wen-ming, MIN Xiao-bo, LI Qing-zhu, WANG Qing-wei, LIU Hui, LIANG Yan-jie, LI Kai-zhong, ZHAO Zong-wen, QU Sheng-li, DONG Zhun-qin. Dissociation mechanism of particulate matter containing arsenic and lead in smelting flue gas by pyrite [J]. Journal of Cleaner Production, 2020, 259: 120875.

[19] KHMELEVA T, SKINNER W, BEATTIE D. Depressing mechanisms of sodium bisulphite in the collectorless flotation of copper-activated sphalerite [J]. International Journal of Mineral Processing, 2005, 76: 43−53.

[20] CHIRITA P, DESCOSTES M, SCHLEGEL M L. Oxidation of FeS by oxygen-bearing acidic solutions [J]. Journal of Colloid and Interface Science, 2008, 321: 84−95.

[21] RADA S, RUS L, RADA M, CULEA E, ALDEA N, STAN S, SUCIU R C, BOT A. Synthesis, structure, optical and electrochemical properties of the lead sulfate−lead dioxide−lead glasses and vitroceramics [J]. Solid State Ionics, 2015, 274: 111−118.

[22] CULEA E, POP L, BOSCA M, RUSU T, PASCUTA P, RADA S. FTIR spectroscopic study of some lead germanate glasses [J]. Journal of Physics: Conference Series, 2009, 182: 012061.

[23] BOYATZIS S C, VELIVASAKI G, MALEA E. A study of the deterioration of aged parchment marked with laboratory iron gall inks using FTIR-ATR spectroscopy and micro hot table [J]. Heritage Science, 2016, 4: 13.

[24] YANG Kun, PENG Hua-bei, WEN Yu-hua, LI Ning. Re-examination of characteristic FTIR spectrum of secondary layer in bilayer oleic acid-coated Fe_3O_4 nanoparticles [J]. Applied Surface Science, 2010, 256: 3093−3097.

[25] WANG Yin-sheng, MURAMATSU A, SUGIMOTO T. FTIR analysis of well-defined α-Fe_2O_3 particles [J]. Colloids and Surfaces A: Physicochemical and Engineering Aspects, 1998, 134: 281−297.

[26] LI Shi-geng, LIU Ru-tie, XIONG Xiang. Preparation and characterization of carbonyl iron soft magnetic composites with magnesioferrite insulating coating layer [J]. Transactions of Nonferrous Metals Society of China, 2020, 30: 3067−3077.

[27] ZHANG Dan, ZHU Ming-yue, YU Jin-gang, MENG Hui-wen, JIAO Fei-peng. Effective removal of brilliant green from aqueous solution with magnetic Fe_3O_4@SDBS@LDHs composites [J]. Transactions of Nonferrous Metals Society of China, 2017, 27: 2673−2681.

[28] PHOLOSI A, NAIDOO E B, OFOMAJA A E. Enhanced arsenic(III) adsorption from aqueous solution by magnetic pine cone biomass [J]. Materials Chemistry and Physics, 2019, 222: 20−30.

[29] WEI Yuan-feng, YU Xing-wen, LIU Cheng-bin, MA Jian-hong, WEI Shu-dan, CHEN Tao, YIN Kai, LIU Hui, LUO Sheng-lian. Enhanced arsenite removal from water by radially porous Fe-chitosan beads: Adsorption and H_2O_2 catalytic oxidation [J]. Journal of Hazardous Materials, 2019, 373: 97−105.

[30] OMWENE P I, ÇELEN M, ÖNCEL M S, KOBYA M. Arsenic removal from naturally arsenic contaminated ground water by packed-bed electrocoagulator using Al and Fe scrap anodes [J]. Process Safety and Environmental Protection, 2019, 121: 20−31.

[31] SANDOVAL M A, FUENTES R, NAVA J L, COREñO O, LI Y, HERNáNDEZ J H. Simultaneous removal of fluoride and arsenic from groundwater by electrocoagulation using a filter-press flow reactor with a three-cell stack [J]. Separation and Purification Technology, 2019, 208: 208−216.

[32] DUBEY A, SINGH S K, TULACHAN B, ROY M, SRIVASTAVA G, PHILIP D, SARKAR S, DAS M. Nano iron pyrite(FeS_2) exhibits bi-functional electrode character [J]. RSC Advances, 2016, 6: 16859−16867.

[33] BIESINGER M C, LAU L W M, GERSON A R, SMART R S C. Resolving surface chemical states in XPS analysis of first row transition metals, oxides and hydroxides: Sc, Ti, V, Cu and Zn [J]. Separation and Purification Technology, 2010, 257: 887−898.

[34] SIRIWARDANE R V, POSTON J A Jr, FISHER E P, SHEN M S, MILTZ A L. Decomposition of the sulfates of copper, iron(II), iron(III), nickel, and zinc: XPS, SEM, DRIFTS, XRD, and TGA study [J]. Applied Surface Science, 1999, 152: 219−236.

[35] SANDSTRÖM Å, SHCHUKAREV A, PAUL J. XPS characterisation of chalcopyrite chemically and bio-leached at high and low redox potential [J]. Minerals Engineering, 2005, 18: 505−515.

[36] LI Fang-xu, ZHOU Xiao-tong, LIN Ri-xiao. Flotation performance and adsorption mechanism of novel 1-(2-hydroxyphenyl)hex-2-en-1-one oxime flotation collector to malachite [J]. Transactions of Nonferrous Metals Society of China, 2020, 30: 2792−2801.

[37] YAMASHITA T, HAYES P. Analysis of XPS spectra of Fe^{2+} and Fe^{3+} ions in oxide materials [J]. Applied Surface Science, 2008, 254: 2441−2449.

[38] DU J, BAO J, LU C, WERNER D. Reductive sequestration of chromate by hierarchical FeS@Fe(0) particles [J]. Water Research, 2016, 102: 73−81.

[39] WANG Zhong-bing, ZHAO Zong-wen, ZHANG Li-feng, LIU Fan-song, PENG Bing, CHAI Li-yuan, LIU Da-chun, LIU De-gang, WANG Tian-yu, LIU Hui, LIANG Yan-jie. Formation mechanism of zinc-doped fayalite($Fe_{2-x}Zn_xSiO_4$) slag during copper smelting [J]. Journal of Hazardous Materials, 2019, 364: 488−498.

[40] YANG Hong-ying, LIU Qian, CHEN Guo-bao, TONG Lin-lin, AUWALU A. Bio-dissolution of pyrite by Phanerochaete chrysosporium [J]. Transactions of Nonferrous Metals Society of China, 2018, 28: 766−774.

[41] KHOSO S, HU Yue-hua, LÜ Fei, GAO Ya, LIU Run-qing, SUN Wei. Xanthate interaction and flotation separation of H_2O_2-treated chalcopyrite and pyrite [J]. Transactions of Nonferrous Metals Society of China, 2019, 29: 2604−2614.

[42] NAVEAU A, MONTEIL-RIVERA F, GUILLON E, DUMONCEAU J. XPS and XAS studies of copper(II) sorbed onto a synthetic pyrite surface [J]. Journal of Colloid And Interface Science, 2006, 303: 25−31.

[43] LIM S, ZHENG Yu-ming, ZOU Shuai-wen, CHEN J. Characterization of copper adsorption onto an alginate encapsulated magnetic sorbent by a combined FT-IR, XPS, and mathematical modeling study [J]. Environmental Science and Technology, 2008, 42: 2551−2556.

[44] ZHAO Chun-xiao, YANG Bao-jun, WANG Xing-xing, ZHAO Hong-bo, GAN Min, QIU Guan-zhou, WANG Jun. Catalytic effect of visible light and Cd^{2+} on chalcopyrite bioleaching [J]. Transactions of Nonferrous Metals Society of China, 2020, 30: 1078−1090.

[45] YAO Li-wei, MIN Xiao-bo, XU Hui, KE Yong, WANG Yun-yan, LIN Zhang, LIANG Yan-jie, LIU De-gang, XU Qiu-jing, HE Yu-yang. Physicochemical and environmental properties of arsenic sulfide sludge from copper and lead-zinc smelter [J]. Transactions of Nonferrous Metals Society of China, 2020, 30: 1943−1955.

[46] KHMELEVA T N, SKINNER W, BEATTIE D A. Depressing mechanisms of sodium bisulphite in the collectorless flotation of copper-activated sphalerite [J]. International Journal of Mineral Processing, 2005, 76: 43−53.

铜冶炼烟气中含砷铜颗粒物的形成与硫酸盐化分解机理

姚文明[1]，闵小波[1,2]，李青竹[1,2]，李开中[1]，王云燕[1]，
王庆伟[1,2,3]，刘 恢[1,2]，曲胜利[3]，董准勤[3]，曲 超[3]，陈 涛[3]，宋 超[4]

1. 中南大学 冶金与环境学院，长沙 410083；
2. 中南大学 国家重金属污染防治工程技术研究中心，长沙 410083；
3. 山东恒邦冶炼股份有限公司，烟台 264109；
4. 烟台恒邦集团有限公司，烟台 264100

摘 要：铜冶炼余热回收锅炉中含有大量的砷铜颗粒物，其砷和铜的原位分离对环境风险控制和有价资源回收至关重要。模拟含砷铜颗粒物的形成，提出黄铁矿原位分解含砷铜颗粒物的新方法，并证实其分解机理。结果表明，在模拟余热锅炉中形成砷含量较高的颗粒物，且以砷酸铜物相为主。黄铁矿促进铜的硫酸盐化，导致砷酸铜的原位分解。在此过程中，砷以气态形式得以释放，从而实现颗粒物中砷和铜的分离。

关键词：铜冶炼烟气；颗粒物；硫酸盐化分解；砷酸铜；黄铁矿

(Edited by Bing YANG)